Melbourne, L. A., Denny, M. W., Harniman, R. L., Rayfield, E. J., & Schmidt, D. N. (2018). The importance of wave exposure on the structural integrity of rhodoliths. *Journal of Experimental Marine Biology and Ecology*, *503*, 109-119. https://doi.org/10.1016/j.jembe.2017.11.007

Journal of Experimental Marine Biology and Ecology 503 (2018) 109–119

Contents lists available at ScienceDirect

Journal of Experimental Marine Biology and Ecology

journal homepage: www.elsevier.com/locate/jembe

The importance of wave exposure on the structural integrity of rhodoliths

Leanne A. Melbourne[a,*], Mark W. Denny[b], Robert L. Harniman[c], Emily J. Rayfield[d], Daniela N. Schmidt[a]

[a] School of Earth Sciences, University of Bristol, Wills Memorial Building, Queens Road, Bristol, (UK), BS8 1RJ
[b] Hopkins Marine Station of Stanford University, Pacific Grove, California, (United States), 93950
[c] School of Chemistry, University of Bristol, Cantock's Close, Bristol, (UK), BS8 1TS
[d] School of Earth Sciences, University of Bristol, Life Sciences Building, 24 Tyndall Avenue, Bristol, (UK), BS8 1TQ

ARTICLE INFO

Keywords:
Material properties
Drag force
Rhodoliths
Finite element analysis

ABSTRACT

The structure (both gross morphology and internal cellular) of rhodoliths (free-living forms of coralline algae) are important factors in the ability of rhodoliths to create complex habitats. Using Finite Element Analysis, models of the internal structure of rhodoliths have been interrogated to assess how changes to the cellular structure affect structural integrity. These models are accurate in their portrayal of the internal skeleton, yet they fail in other ways. Specifically, they lack accurate environmental loads and material properties (Young's modulus), which form the basis of an accurate quantification of the structural integrity of rhodoliths. Here we measure the material properties of rhodoliths and quantify the hydrodynamic forces acting on them. Applying correct material properties and hydrodynamic forces, our results show that rhodoliths experience larger stresses than previously modelled. Water velocities representing storm surges cause internal stresses exceeding experimentally derived breakage stresses. As the intensity and frequency of storm surges are predicted to increase, the forces generated by them will result in breakage and hence affect their role as habitat builders.

1. Introduction

Rhodoliths, free-living non-geniculate (lack of non-calcified sections) coralline algae, are important habitat formers in the shallow marine environment, due to their densely branched 3D structure (Fig. 1). The aggregation of rhodoliths creates structurally and functionally complex beds that support a high level of biodiversity (Biomaerl, 1999), including commercial important species of scallops and fish larvae (Biomaerl, 1999; Kamenos et al., 2004).

Rhodoliths are coastal ecosystem engineers. Their morphology and subsequently bed distribution are highly affected by the coastal environment. In a latitudinal transect, it has been shown that changes in size, branch thickness and rhodolith shape mainly occur geographically than between species (Carro et al., 2014). Additionally, morphology can change within the same beds. For instance, rhodolith volume and branching density generally decreases with water depth (Bahia et al., 2010; Steller and Foster, 1995). Temperature and light are both first order environmental factors known to control rhodolith bed distribution (Foster, 2001), with substrate and hydraulic energy acting as a secondary control (Bosence and Pedley, 1982). For rhodoliths water flow must be within optimal ranges for growth. Too slow and rhodoliths are smothered by silt, but too fast and rhodoliths are susceptible to breakage (Foster, 2001). Rhodolith breakage can lead to the formation of coralline gravels (Bosence and Pedley, 1982). Rhodolith beds in Brittany, France are found in areas where mean current velocity ranges from 0.02 to 0.73 m s^{-1}, with the lowest percentage of rhodolith cover (< 59% covered) occurring in areas of water velocities exceeding 0.50 m s^{-1} (Dutertre et al., 2015). How often a rhodolith turns, due to water motion or bioturbation, is a factor that controls rhodolith shape, as a decrease in turning leads to more discoidal rather than spheroidal shapes (Steller and Foster, 1995). On the other hand rhodolith movement is important for survival. In general, the reduction in turning through decreasing wave-induced water velocity with depth or distance from land can reduce the size of rhodolith beds (Steller, 1993). This pattern can be reversed when more optimal conditions occur further away from land, due to environmental factors such as sedimentation, salinity and nitrate concentration also affecting bed distribution (Amado-Filho et al., 2007; Dutertre et al., 2015; Steller and Foster, 1995).

Rhodolith internal structure and material properties, which affect structural strength, are also affected by environmental conditions. Cellular structure changes to form larger cells with thinner cell walls in response to experimentally elevated temperature and CO_2 levels (Ragazzola et al., 2012). Finite element (FE) simulations demonstrate

* Corresponding author.
E-mail address: l.melbourne@bristol.ac.uk (L.A. Melbourne).

https://doi.org/10.1016/j.jembe.2017.11.007
Received 30 June 2017; Received in revised form 19 November 2017; Accepted 20 November 2017
Available online 17 March 2018

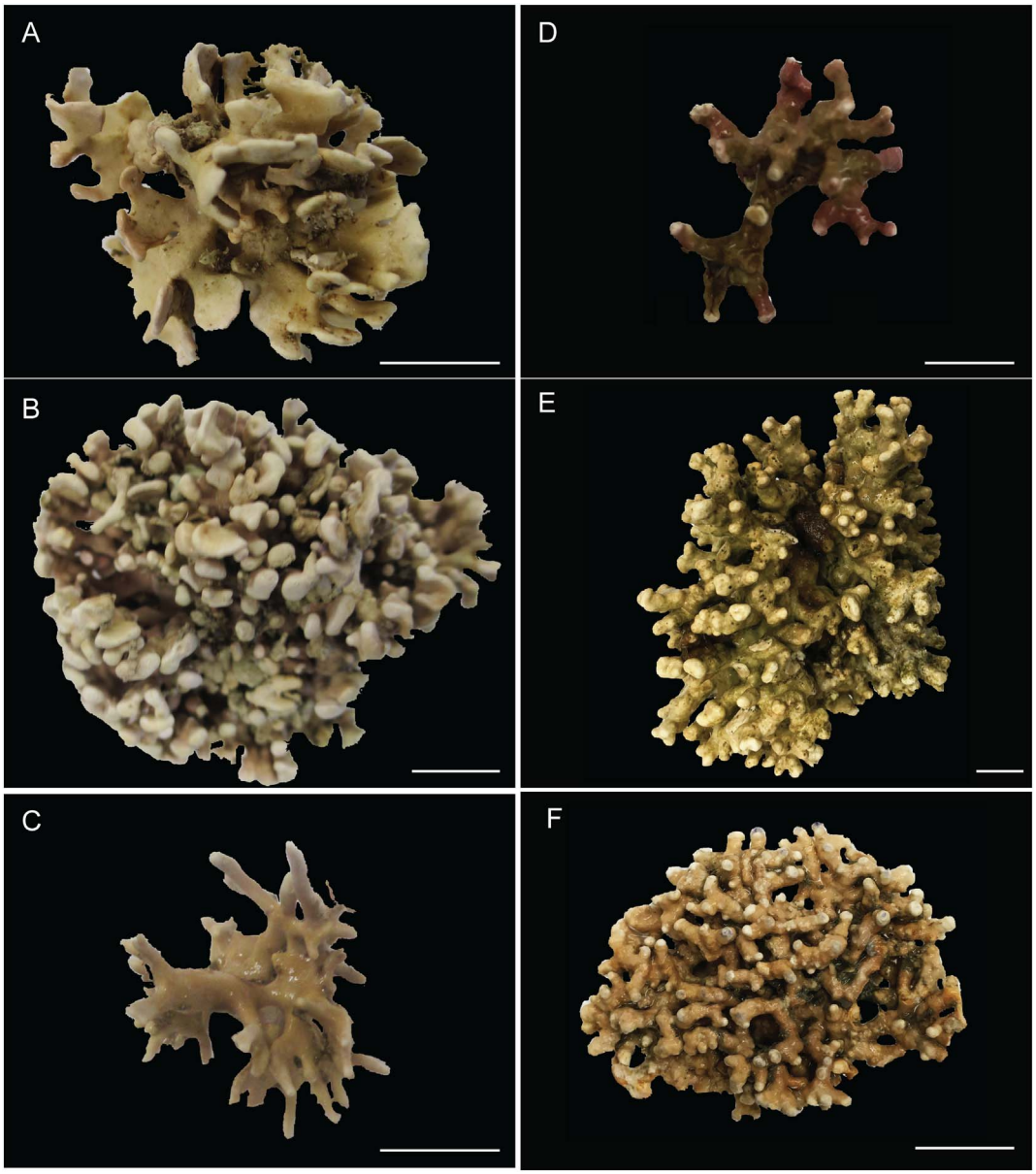

Fig. 1. Rhodoliths of varying morphologies of *Lithopyllum margaritae* (A–C) and *Phymatolithon calcareum* (D–F). Open branched (D), Spheroidal (E) and discoidal (F). Scale bar 1 cm.

that these growth changes reduce the structural integrity of the rhodolith, potentially making it more susceptible to breakage (Melbourne et al., 2015; Ragazzola et al., 2012). It is important to note that a longer exposure of 10 months resulted in acclimation of the organism and growth in the experimental material similar to control specimens (Ragazzola et al., 2013). Rhodoliths form high Mg-calcite skeletons (Moberly, 1968) and the amount of magnesium (Mg) in the skeleton is also affected by the environment (Halfar et al., 2000; Kamenos et al., 2008). Warmer temperatures result in a higher incorporation of magnesium into the skeleton compared to the colder winter temperatures creating alternating bands of high and low magnesium. Increasing CO_2 levels are suggested to reduce Mg incorporation resulting in the loss of this distinct banding (Ragazzola et al., 2013; Ragazzola et al., 2016). On the other hand, one study has shown how future CO_2 conditions have had no effect on the Mg incorporation of rhodoliths (Kamenos et al., 2013). Changes in Mg content are thought to affect the hardness of calcite in echinoderms, as higher concentrations of Mg lead to a harder material (Wang et al., 1997). These structural and material changes therefore have the potential to affect rhodolith structural integrity and ecosystem function.

Finite element models based on the internal growth structure of rhodoliths are ideal to assess their structural integrity (Melbourne et al., 2015; Ragazzola et al., 2012). However, in order to make meaningful predictions in quantifying the risk of possible breakage, FE simulations need to incorporate accurate rhodolith material properties and use hydrodynamic forces and water velocities that rhodoliths are exposed to. Fragmentation is the main form of rhodolith propagation (Irvine and Chamberlain, 1994). However, smaller fragments are more susceptible to smothering by silt (Hall-Spencer and Moore, 2000; Wilson et al., 2004), while rhodolith beds composed of smaller fragments will alter the composition of the associated fragments (Grall and Hall-Spencer, 2003). Given the importance of rhodolith size, wave exposure on rhodolith movement and morphology (Marrack, 1999; Scoffin et al., 1985; Steller and Foster, 1995) and the likelihood of more intense and frequent storm surges under climate change (Elsner et al., 2008; Knutson et al., 2010), it is paramount to quantify these hydrodynamic forces and the breakage limits of rhodoliths.

The aim of this study is to quantify the material properties (breaking stress, Young's modulus) and drag coefficients for varying morphologies of rhodoliths from Falmouth, UK and the Gulf of California, Mexico.

Drag coefficients provide a greater understanding of the forces these organisms experience. We chose these two sites to assess whether there is a difference in the drag coefficients acting on rhodoliths from different environmental regions (temperate vs subtropical). Skeletal and material properties, along with accurate hydrodynamic forces, inform our tailor made Finite Element models and enable us to estimate how the structural integrity of rhodoliths will be affected by future ocean conditions. With this information we can make a more informed decision on how rhodoliths and the habitat(s) they provide will be affected by future global change.

2. Materials and methods

2.1. Samples

The dominant species from each site were used in the experiments (Irvine and Chamberlain, 1994; Riosmena-Rodriguez et al., 1999). *Lithothamnion corallioides* (P.Crouan & H.Crouan) P.Crouan & H.Crouan and *Phymatolithon calcareum* (Pallas) W.H.Adey & D.L.McKibbin were collected from *St* Mawes Bank, Falmouth in July 2013. *Lithophyllum margaritae* (Hariot) Heydrich from the Gulf of California, Mexico was collected in 2007 (Table 1).

2.2. Calculating rhodolith breakage stress

Material's strength is measured as breaking stress, defined as the maximum stress a material can stand before it breaks. Here we use beam theory to translate the force applied to a piece of rhodolith skeleton into the stress imposed within the material (σ_{brk}). Bending a beam of known length informs us how beam shape interacts with an applied moment to impose stress on the material of the beam (Eq. 1).

$$\sigma_{brk} = (My)/I \quad (1)$$

where M (Nm) is the bending moment of the beam, y (m) is the distance to the neutral surface (the area where the beam is unstrained) and I (m^4) is the second moment of area (a descriptor of the beam's cross sectional shape) (Young and Budynas, 2002).

Branches of *P. calcareum* were cut and polished down to thin rectangular beams, using a Dremel tool and sandpaper. *P. calcareum* was used as the branches were sufficiently thick to create beams large enough for analysis. Beams were placed lengthways into a custom made tensometer and attached using wax (Martone, 2006). The tensometer was used to perform a three-point bending test. A concentrated force is applied to the centre of beam (x), which is supported at two points (z) with a known length of 6.7 mm (Fig. 2A). A small bar was used to apply the force until the beam cracked. A force transformer (LVDT; model 100HR, Schaevitz Engineering, Pennsauken, New Jersey) was used to measure the bending of a beam and thereby the corresponding voltage applied by the bar was calculated.

To calculate I the cross section of the broken beam was imaged and measured using ImageJ software (Rasband, 1997–2011) (Fig. 2B) (Eq. 2).

$$I = d^3 (a^2 + 4ab + b^2)/36 (a + b) \quad (2)$$

where a (m) is the short length of the beam, b (m) is the longer length of the beam and d (m) is the height of the beam perpendicular to b. The tenseometer was calibrated using known weights (kg). Weights ranging from 0.1 kg up to 1.5 kg were weighed on the tensometer and the corresponding voltages were measured.

Weight (N) vs voltage was plotted and the gradient of the resulting line was used to convert voltages required to break algal beams into forces.

The bending moment, M (Nm), applied to the test beam was calculated using Eq. 3.

$$M = \frac{1}{2} \times F \times \textit{lever arm} \quad (3)$$

where F is the force (N) and the lever arm is the length of the beam covering the hole in the tenseometer (6.7 mm).

A linear regression was performed to assess the relationship between force (N) and breaking stress.

Breaking stress (σ_{brk}) was subsequently calculated using Eq. 1.

2.3. Estimating wave velocities

To assess the effect of substrate and rhodolith morphology on movement, unattached rhodoliths of various sizes and morphologies (Fig. 1A–F) were placed in a recirculating water flume, 43 cm in both height and width (Martone et al., 2012), on different substrates; glass, sandpaper and a Lego obstacle course. These substrates were chosen to compare rhodolith movement between sand (sandpaper) and in a rhodolith bed (Lego obstacle course). Glass was used as a control to quantify how rhodoliths move when substrate does not impact movement. For glass, velocity was increased until rhodoliths started to move (as there was no obstacle to hinder movement). For the sandpaper and the Lego obstacle course velocity was increased until the rhodolith completed the course, with the highest velocity recorded. The sandpaper had a length of 23 cm, while the Lego obstacle course had a length of 20 cm.

Large, rounded rhodoliths were put through a barrier test consisting of the same Lego course at two different heights, the first obstacle 2 cm (8 cm from the start of the course) and a second 3 cm high (12 cm from the start of the course). Velocity was increased until both jumps were completed. All other rhodolith morphologies were too small to traverse the barrier and hence were not used in the experiments.

The recirculated flume operates in RPM. As water velocities are not constant throughout the water column, large and small rhodoliths will experience slightly different water velocities. To account for this water velocities were calculated at two different heights, within the flume, using the Sontek acoustic doppler velocimeter (ADV Vectrino, Nortek, Rud, Norway). The velocimeter uses the principle of the doppler shift to measure the water velocity in three dimensions, which allows rpms to be converted into water velocities using the size-dependent calibrations derived from the velocimeter.

To assess if substrates and morphologies were statistically significant in affecting rhodolith movement a nested ANOVA with Satterthwaite approximation (Satterthwaite, 1946) was performed in Excel.

Table 1
Information on the collection of the three species, *Lithothamnion corallioides*, *Phymatolithon calcareum* and *Lithophyllum margaritae* used in the experiments and which experiments they were a part of.

Species	Location	Year	Depth range (m)	Breakage experiments	Water velocity experiments			Drag coefficients
					Glass	Sand	Lego	
Phymatolithon calcareum	Falmouth, UK	2014	3.9–7.5	X	x	x	x	x
Lithothamnion corallioides	Falmouth, UK	2014	3.9–7.5		x	x	x	x
Lithophyllum margaritae	Gulf of California, Mexico	2007	2–11					x

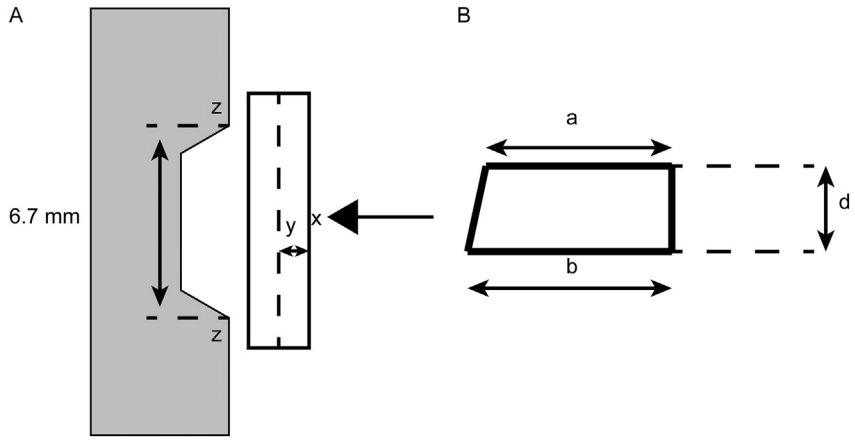

Fig. 2. A Schematic diagram of the algal beam in the tensometer with measurements used to calculate breaking stress, B the cross section of the broken algal beam with measurements used to calculate breaking stress.

2.4. Calculating drag coefficients

The primary hydrodynamic force exerted on marine macroalgae is drag, which acts in the direction of flow (Carrington, 1990). Drag force (F_{drag}) can be calculated as follows

$$F_{drag} = \frac{1}{2}\rho\nu^2 A C_d \quad (4)$$

where ρ is the density of seawater (1025 kg m^{-3}), ν is the water velocity (m s^{-1}), A is the projected area in the direction of flow (m^2) and C_d is the dimensionless drag coefficient (Carrington, 1990).

Rhodoliths (*Phymatolithon calcareum*, *Lithothamnion corallioides* and *Lithophyllum margaritae*) were dropped into a cylindrical tube (10.7 cm in diameter) filled with water. Velocities were calculated by measuring the time (s) it took for the rhodolith to drop between two points of known height (1.27 m) when the specimens were no longer accelerating through the water column.

The orientation to flow impacts calculated drag coefficients (3.3). Hence some rhodoliths with a flat, discoidal morphology were also dropped again with tied lead weights to orientate them in the way they would be naturally orientated against flow.

Drag coefficients were calculated as follows:

$$C_d = 2F/(\rho\nu^2 A) \quad (5)$$

where C_d is the drag coefficient, F is the weight of the rhodolith in water (N) (to account for buoyancy), ρ is water density (1000 kg m^{-3}), ν is rhodolith velocity (m s^{-1}) and A is the algal area projected to flow (m^2). Water density was used instead of seawater density as the experiments were done in freshwater.

The area subjected to flow was calculated by taking an image of the underside of the falling rhodolith and using the threshold tool in ImageJ analysis software to isolate and measure the rhodolith surface area (Rasband, 1997–2011).

2.5. Estimating forces

Forces were estimated at given water velocities using calculated drag coefficients (C_d) and measured planform areas (A) (Eq. 4).

2.6. Material properties

The nanoscale surface morphology and Young's Moduli of both summer and winter growth of *Lithothamnion glaciale* Kjellman and *Phymatolithon calcareum* were determined using atomic force microscopy (AFM). A multi-mode VIII AFM with Nanoscope V controller and PeakForce control mechanism were utilised. The force-curves measured for means of set-point control in the PeakForce system can be analysed in real-time to provide quantitative nanomechanical mapping (QNM). QNM was conducted with Nusense SCOUT cantilevers [NuNano, Bristol, UK], nominal tip radius 5 nm and spring constants in the range 21–42 N m^{-1}. The system was calibrated for measurement of Young's modulus fitting with DMT models, using the relative method and a sample of highly oriented pyrolytic graphite (HOPG) with known Young's modulus of 18 GPa. Young's moduli measured by this method are representative of the Young's modulus at the surface measured. The results are likely to relate to the macro-scale Young's modulus of the material under strain, but does not involve compression of the entire sample, as deformation is restricted to a few nanometers in depth.

Individual branches were embedded in epoxy resin, EpoThin. Each sample was polished with a series of silicon carbide grinding papers to expose the internal structure of the thallus. Diamond pastes were used to produce a finer polish and samples were then sonicated in ethanol to remove dislodged calcite. Regions at the centre-point furthest from the resin-sample interface were investigated. The surface morphology was first imaged and ensured clean of resin contamination on each sample utilising SCANASYST-AIR-HR cantilevers, tip radius 2 nm, and a high-speed scan unit. It is unlikely that macro-scale structure i.e., bending of branches of different thickness influence surface measurements at the micron scale with nanoscale deformation. However, to ensure that macro-structure did not influence surface measurements, the intersections between four different cells was analysed (Fig. S1A–D).

2.7. Finite element analysis

We build the analysis on the existing models of Melbourne et al. (2015) using realistic material properties and hydrodynamic forces determined in this study to understand the pressures experienced by these organisms. Finite element analysis is a mathematical technique originally used in engineering to assess stress (σ), strain (ε) and deformation in structures (Zienkiewicz et al., 2005). FEA transforms a continuous structure into a discrete number of elements connected to each other via nodes, known as the mesh. Young's modulus (Σ) and Poisson's ratio (σ) are applied to provide the structure's elasticity. Once constraints and the magnitude and direction of loads are applied, strain is calculated through node displacement. Stress is subsequently calculated using the Young's modulus (Eq. 6). (For mathematical equations see Mathematics of FEA: Rayfield, 2007; Supplement).

$$\Sigma = \sigma / \varepsilon \quad (6)$$

The methods for creating and analysing the model are detailed in Melbourne et al. (2015). The model represents a geometric approximation of a cube of rhodolith skeleton of dimension 80 μm × 80 μm × 80 μm, with a Young's modulus of 36 GPa and an applied loading pressure of 20,000 Pa (Melbourne et al., 2015). This

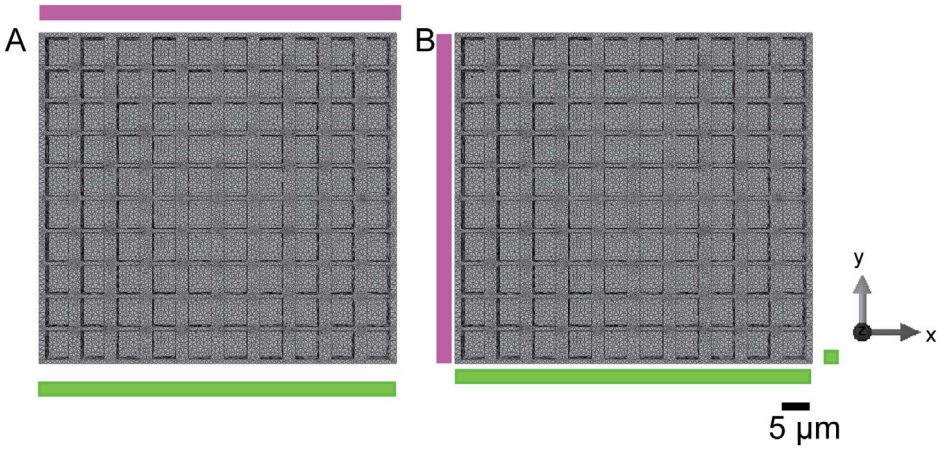

Fig. 3. The loading types used in the Finite Element models in compression (A) and shear (B). Bars represent loading and constraints; Loads – pink, constraints – green. Scale bar 5 μm. (For interpretation of the references to colour in this figure legend, the reader is referred to the web version of this article.)

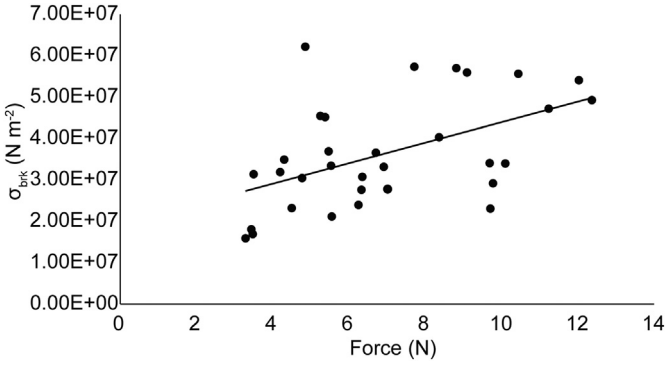

Fig. 4. Force (N) vs breaking stress (N m^{-2}) acting on beams of *Phymatolithon calcareum* used in the experiments.

geometric FE-model captures the patterns of stress and strain within a natural rhodolith skeletal cube of the same dimensions, however realistic loading conditions were unknown. Here using our newly quantified wave velocities, we revise the loading conditions in the FE-model to a load force of 0.03 N, characteristic of a wave velocity of 0.40 m s^{-1} (Section 3.3) and an elastic modulus of 19.37 GPa, representative of a summer band of *Phymatolithon calcareum* (see Section 3.1). Future climate change predictions estimate higher likelihood of storm surges impacting coastal ecosystems. We used models run with loads of 4 N (load calculated for a wave velocity of 5 m s^{-1}) to simulate these situations (Section 3.3).

Two loading types were applied to both models: compression (Fig. 3A) and shear (Fig. 3B). The shear loading type had a small constraint applied to the opposite face of the load to enable the model to run (Fig. 3B). Von Mises stress, strain energy and maximum principal stress were recorded. We applied maximum principal stress theory, a useful tool for predicting failure in brittle materials. It states that failure will occur when the maximum principal stress exceeds the yield maximum strength in tension at the elastic limit. We report the 95th percentile for von Mises and maximum principal stress to exclude the extreme erroneous stresses caused by elements adjacent to the loads and constraints. All 3D geometric models were created and analysed in the Finite Element software package, Abaqus/CAE, v.6.14, (Simula, USA, Dassault Systémes, //Simula, Providence, RI, USA).

3. Results

3.1. Structural and material properties of rhodoliths

The average breaking stress (σ_{brk}) of *Phymatolithon calcareum*, is 36.39 ± 2.31 MPa (mean ± SE) and the breaking force of *P. calcareum* is 6.95 ± 0.47 N (mean ± SE). The relationship between force and breaking stress is linear (Linear regression $R^2 = 0.257$, $F_{1,32} = 10.44$, $p < 0.01$) (Fig. 4).

In both species, there is a clear difference in the Young's modulus (E) between summer and winter growth of both *P. calcareum* and L. *glaciale*. The Young's modulus of the winter band (E = 25.24 GPa;

Table 2
Rhodolith hydrodynamic performance indicators, averages ± S.E. (ranges).

	Number of specimens	Water velocities that are required to get rhodoliths moving (m s^{-1})			Jumping barrier heights (m s^{-1})		A (m^2)	Drag Coefficient
		Glass	Sand	Lego	2 cm	3 cm		
Discoidal (IV)	3	0.255 ± 0.02 (0.2–0.3)	0.361 ± 0.03 (0.3–0.42)	0.5994 ± 0.04 (0.51–0.66)			4.8×10^{-4}	1.18 ± 0.02 (1.14–1.2)
Discoidal (IV) vertically orientated	4						3.4×10^{-4}	0.72 ± 0.02 (0.66–0.76)
Open branched (II)	10	0.287 ± 0.02 (0.27–0.32)	0.358 ± 0.03 (0.22–0.51)	0.579 ± 0.03 (0.46–0.8)			3.4×10^{-4}	0.62 ± 0.02 (0.41–0.88)
Spheroidal (IV)	5	0.333 ± 0.02 (0.3–0.42)	0.365 ± 0.02 (0.3–0.49)	0.493 ± 0.03 (0.39–0.56)	0.505 ± 0.01 (0.46–0.53)	0.893 ± 0.05 (0.84–1.06)	3.5×10^{-3}	1.21 ± 0.13 (0.85–1.64)
Lithophyllum margaritae	30						6.2×10^{-4}	0.64 ± 0.02 (0.38–0.96)
All rhodoliths	44						5.4×10^{-4}[a]	0.64 ± 0.02[a] (0.38–0.96)

[a] Average does not include spherical rhodoliths and includes discoidal rhodoliths in a vertical orientation.

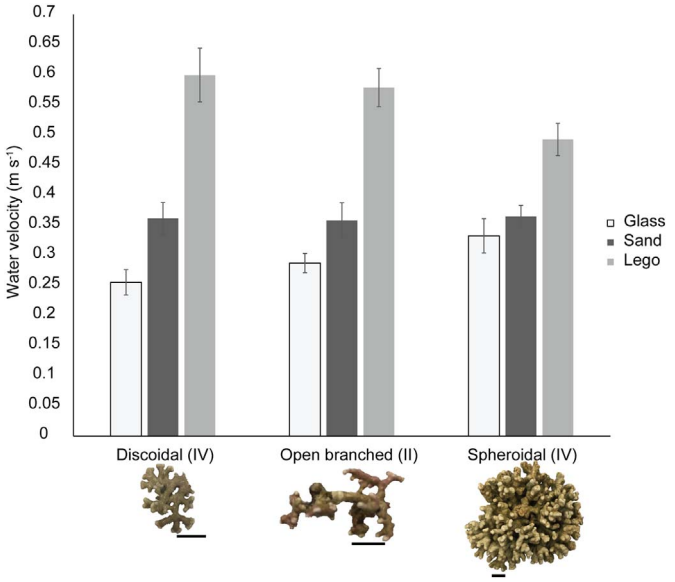

Fig. 5. Water velocities (m s^{-1}) of the three different shapes of rhodoliths (Discoidal, open branched and spheroidal) on different substrates. Scale bar 1 cm.

E = 28.85 GPa respectively) is higher than the summer band (E = 19.37 GP; E = 23.02 GPa respectively).

3.2. The relationship between rhodolith morphology, substrate and water velocity

To assess the impact of substrate on rhodolith movement we measured the water velocities required to initiate *P. calcareum* and L. *corallioides* rhodoliths movement on different substrates. Water velocities between 0.2 and 0.8 m s^{-1} are required to move rhodoliths of differing morphologies along all substrates (glass, sand and Lego). All rhodoliths slide along glass whereas on sand and Lego, all rhodoliths roll. The lowest water velocities to enable movement are required on glass (0.292 ± 0.02 m s^{-1}); the highest water velocities are required for the Lego course (0.555 ± 0.02 m s^{-1}) while for sand the average water velocity is 0.361 ± 0.02 m s^{-1}. The differences in the water velocities between all three substrates are significant (Nested anova F(1,47) = 37.2, $p < 0.01$). There are no species specific differences in the water speed causing movement.

Consequently, *P. calcareum* and *L. corallioides* rhodoliths are grouped based on morphology and not by species. These are 1) small, flat compact rhodoliths, 2) small rhodoliths with long protuberances and 3) large round rhodoliths (Fig. 1 & 5). Using Bosence (1976) morphological diagram, which categorises rhodoliths based on shape, the three groups will now be referred to as 1) discoidal (IV), 2) open branched (II) and 3) spheroidal (IV); where the roman numerals refer to degree of branching. On glass, spheroidal rhodoliths require larger water velocities compared to discoidal and open branched rhodoliths (0.333 ± 0.02 m s^{-1}; 0.255 ± 0.02 m s^{-1} and 0.287 ± 0.02 m s^{-1} respectively) (mean ± SE). On sand movement of all rhodolith morphologies is caused by water velocities which are within error of each other (Table 2). In the Lego course, discoidal and open branched rhodoliths became stuck within the obstacle course and therefore require higher water velocities to become unstuck. Hence both discoidal and open branched rhodoliths require the largest velocities to complete the Lego obstacle course (0.599 ± 0.04 m s^{-1}; 0.579 ± 0.03 m s^{-1} respectively), while the more compact spheroidal rhodoliths require the smallest water velocities to complete the course (0.493 ± 0.03 m s^{-1}). (Table 2, Fig. 5). However, the differences in the water velocities between the morphological groups, for each substrate, are not statistically significant (Nested anova F(1,47) = 1.23, $p = 0.31$).

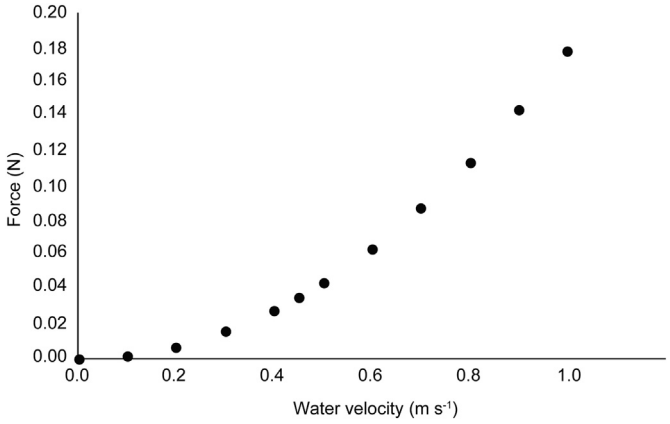

Fig. 7. Water velocity (m s^{-1}) vs drag force (N) of all rhodoliths.

In the barrier test, spheroidal rhodoliths require higher water velocities to jump a barrier 3 cm high compared to a barrier 2 cm high (0.892 ± 0.05 m s^{-1}; 0.505 ± 0.01 m s^{-1} respectively). However, depending on rhodolith momentum i.e., how quickly the rhodolith moved, rhodoliths are able to occasionally traverse the second higher hurdle at the same water velocities as the first hurdle (Table 2).

3.3. Forces experienced by rhodoliths

Drag coefficients are calculated at water velocities corresponding to a range of Reynolds numbers (*Re*) between 3.8×10^3 and 2.7×10^4. Algal planform area and drag coefficient are linearly related (Linear regression $R^2 = 0.496$; F1, 46 = 46.34, $p < 0.01$) (Fig. 6A). A weaker linear relationship is found once spheroidal rhodoliths are removed and discoidal rhodoliths are orientated vertically (Linear regression $R^2 = 0.206$; F1, 42 = 10.62, $p < 0.01$) (Fig. 6B). Drag coefficients range from 0.38 to 1.64 (Table 2). Discoidal and spheroidal rhodoliths have drag coefficients higher than 1 (spheroidal rhodoliths – 1.21 ± 0.13; discoidal rhodoliths – 1.18 ± 0.02), while open branched rhodoliths have average drag coefficients of 0.62 ± 0.05. Vertically orientating discoidal rhodoliths decreased the drag coefficients to 0.72 ± 0.02. The drag coefficients of *Lithophyllum margaritae*

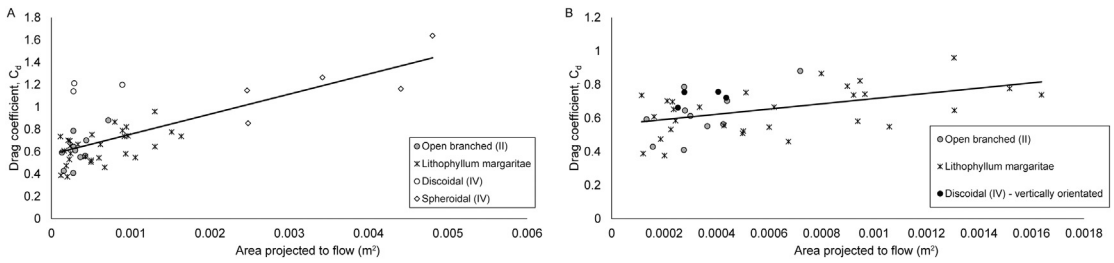

Fig. 6. Drag coefficient vs projected area (m^2). Plot with all rhodoliths (A). Plot with discoidal rhodoliths vertically orientated and excluding spheroidal rhodoliths (see text for discussion) (B).

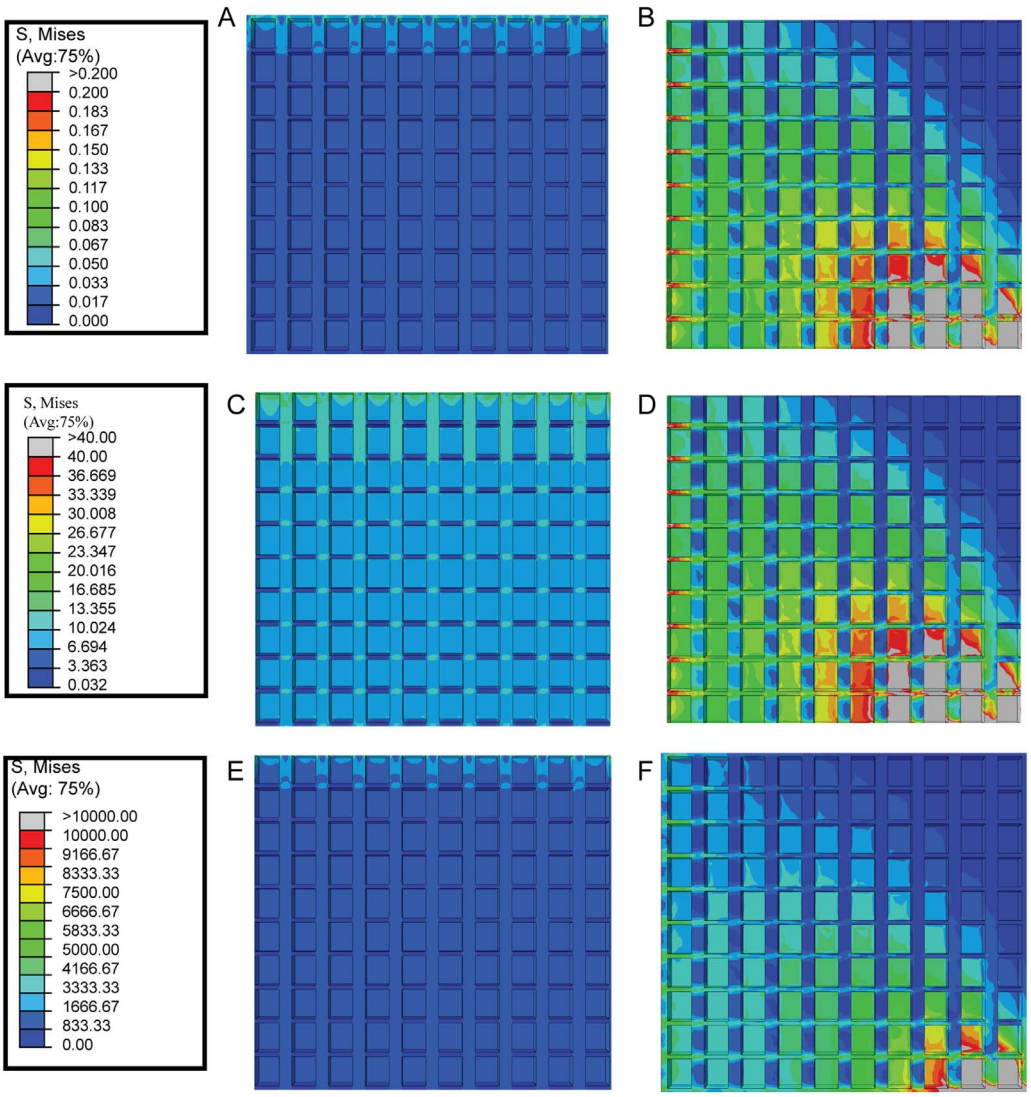

Fig. 8. Finite element von Mises stress maps of the old model published by Melbourne et al. (2015), load 20 GPa (A–B); von Mises stress maps of the new model with accurate material properties with a load of 0.03 N (C–D); and the same model under loads predicted for a storm surge, load 4 N (E–F). Compression loadings (A, C & E) and shear loading (B, D & F). Units – MPa.

specimens did not clearly separate out based on morphology, hence for ease they were kept as one taxonomic group. This lack of morphological difference was also the reason why L. *margaritae* specimens were not used in the water velocity experiments as it was shown in 3.2 that rhodolith morphology did not significantly affect rhodolith movement (see discussion for details).

Drag forces are calculated using an average drag coefficient and algal area projected to flow for all rhodoliths (Fig. 7). Spherical rhodoliths were excluded as drag coefficients were overestimations (see discussion), and discoidal rhodoliths included were vertically orientated. Drag forces for wave velocities up to 1 m s^{-1} reach up to 0.18 N. On a 1–3 m deep reef platform, organisms can experience wave velocities from 1 m s^{-1} up to 5 m s^{-1} (currently expected during a tropical cyclone) (Madin, 2004). Using a velocity of 5 m s^{-1}, rhodoliths experience a corresponding force of 4 N.

3.4. Refined model analysis

Using drag forces and material properties derived in this study, the new more accurate FE-model display larger stresses (von Mises and max principal) and strains than the previous model (Fig. 8A–D; Table 3). For both models, stresses and strains are larger under shear loading compared to compression loading (Fig. 8A–D; Table 3). Under compression loading the stress distributions between the two models differ. Higher stresses are associated with cell nodes throughout the new model, which are not evident in the old model (Fig. 8A, C). Under shear loading a similar stress distribution is displayed in both models with lower stresses on the inter cell walls compared to the intracell walls (Fig. 8B, D).

The total von Mises stress for the new models, testing realistic wave loadings, are two orders of magnitude greater than the old model (old compressive – 1.85E + 05 MPa; old shear – 3.10E + 05 MPa; new compressive – 4.5.3E + 07 MPa; new shear – 8.19E + 07 MPa). The largest difference between the old and new model is in the total strain energy (old compressive – 4.35E-03 pJ; old shear – 2.58E-02 pJ; new compressive – 4.84E + 02 pJ; new shear – 3.35E + 03 pJ). Increasing the load to 4 N simulating storm in shallow water (see Section 3.3) increases the total von Mises stress (compression – 6.050E + 09 MPa; shear – 1.09 + E + 10 MPa) by two orders of magnitude and the total strain energy by four orders of magnitude compared to the improved model under current loading conditions (compression – 8.61E + 06 pJ; shear – 5.96E + 07 pJ). The stress distributions under shear and compression loadings for the model under a 4 N load are similar to the model under a 0.03 N load (Fig. 8C–F). For a full list of all stresses and strain energies see Table 3.

Table 3
Rhodolith Finite element model performance. Comparison with Melbourne et al. (2015) model to models presented here with experimentally determined material property and wave loading input parameters.

		Strain energy (pJ)	Von mises stress (MPa)	95% percentile von mises stress (MPa)	Stress max principal (MPa)	95th percentile max principal stress (MPa)
Melbourne et al. (2015) FE-model (load 20 GPa)	Compression	4.35E − 03	1.85E + 05	3.91E − 02	1.18E + 04	8.95E − 03
	Shear	2.58E − 02	3.10E + 05	1.32E − 01	7.11E + 04	3.94E − 02
New FE-model (load 0.03 N)	Compression	4.84E + 02	4.53E + 07	9.56E + 00	2.88E + 06	2.19E + 00
	Shear	3.35E + 03	8.19E + 07	3.50E + 01	1.88E + 07	1.04E + 01
New FE-model (load 4 N)	Compression	8.61E + 06	6.05E + 09	1.27E + 03	3.84E + 08	2.92E + 02
	Shear	5.96E + 07	1.09E + 10	4.66E + 03	2.51E + 09	1.39E + 03

4. Discussion

4.1. The relationship between form and flow

Rhodoliths are very plastic in their form. This plasticity has often been related to their habitat (Carro et al., 2014), though accurate quantification of the relationship was missing. Our results are the first quantification of hydrodynamic forces on rhodoliths. Drag coefficients for rhodoliths are on average larger than calculated drag coefficients for most fleshy macroalgae (0.1–0.3) (Carrington, 1990; Dudgeon and Johnson, 1992; Gaylord et al., 1994) and geniculated coralline algae (0.1–0.3) (Martone and Denny, 2008). However, comparing drag coefficients at similar velocities used in this study fleshy macroalgae can have much larger drag coefficients (up to 0.75, as seen for *Pelvtiopsis limitata*) (Gaylord et al., 1994). Both fleshy macroalgae and geniculated corallines are able to rearrange their shape in flow (Vogel, 1984), which enables these organisms to be more streamlined than rhodoliths, and hence have lower drag coefficients. This reconfiguration ability also results in drag coefficients that are inversely proportional to water velocity for fleshy macroalgae and the geniculated corallines, whereas rhodoliths being 'bluff bodies' have constant drag coefficients at these water velocities (Fox et al., 1985; Gaylord et al., 1994). This flexibility enables fleshy macroalgae to withstand larger water velocities as the reduction in drag coefficient leads to a lower force exerted on these organisms. Rhodoliths with constant drag coefficients will inevitable experience larger forces under increasing storm surges, making it harder to fulfil their ecosystem function.

The drag coefficients for spheroidal rhodoliths are roughly 70% larger than any other rhodolith form, which is a result of their large ratio of frontal area to volume, similar to branching corals (Samuel and Monismith, 2013). The area exposed to flow used to calculate drag coefficients typically represents the external surface. Rhodoliths and branching corals, though, additionally have internal branches that are exposed to flow, which are not accounted for in the calculated projected area (Eq. 5). Hence the projected area used in the calculation is smaller than the actual projected area subjected to flow, leading to an overestimation of the drag coefficient. Discoidal rhodoliths also have large drag coefficients, but once orientated vertically through the water column the discoidal rhodoliths have drag coefficients comparable to the other rhodoliths in this study. The established drag coefficients are similar to the stony reef forming coral *Acroporia reticulata* (Vosburgh, 1982) and some marine invertebrates such as the predatory snail *Thais canaliculata* (Denny, 2016). Consequently, the shape of the rhodolith does not have a strong control on drag coefficients and drag forces exerted on rhodoliths are dependent on just size and water velocities.

At Reynolds numbers around 10^4 drag coefficient should be constant and not influenced by projected area, yet we see a significant linear relationship albeit with little explanatory power. This relationship is still apparent, though weaker, when spheroidal rhodoliths were excluded and discoidal rhodoliths vertically oriented due to the above discussed reasons. However, the root mean squared error for this relationship is similar to the root mean squared error of a line describing a constant drag coefficient and therefore does not allow us to reject or accept either hypothesis. Smaller rhodoliths experiencing lower Reynolds numbers are likely the cause for the weak but positive linear relationship. Drag coefficients for geniculated corallines decreases with increasing projected area (Martone and Denny, 2008), also a consequence of their reconfiguration ability as larger fronds have a larger ability to reconfigure against flow. The lack of relationship between drag coefficient and projected area highlights yet again the inability of rhodoliths to reconfigure against flow in order to reduce the forces exerted on them. As a result rhodoliths are unable to inhabit the more dynamic parts of the coast where fleshy macroalgae and geniculated corallines are present.

Their inability to reconfigure their shape causes water velocity to have a greater impact on shaping rhodolith morphology through movement, but also by limiting the forms that can be expressed. Substrate influences rhodolith movement. Our results show that wave velocities between 0.2 and 0.51 m s^{-1} result in movement of rhodoliths on glass and sandpaper. When rhodoliths interact with the substrate and obstacles, higher velocities (between 0.39 m s^{-1} and 0.8 m s^{-1}) are required to initiate movement again. In the field threshold velocities between 0.3 m s^{-1} and 0.4 m s^{-1} (Scoffin et al., 1985) on sand and oscillating currents between 0.25 m s^{-1} and 0.35 m s^{-1} on a rhodolith bed (Marrack, 1999) were required to initiate rhodolith movement, whereas rhodoliths nestled in with other rhodoliths in currents up to 0.37 m s^{-1} never moved (Marrack, 1999). The stability of nested rhodoliths suggest that the core of a maerl bed can withstand much larger energies than the fringes, which would erode away more easily when wave energy increases. Our laboratory based results corroborate the field data. Our results also show how substrate has more of an influence on rhodolith movement than morphology. Rhodoliths found on sand, where the rhodolith bed itself is very shallow, are more likely to be spherical as they would experience more movement than a rhodolith on top of a dense bed (Steller and Foster, 1995).

4.2. The impact of geochemical changes on material properties

Material properties in *Phymatolithon calcareum* and *Lithothamnion glaciale* vary between summer and winter growth, with lower Young's modulus for tissue deposited in the warmer summer months (winter bands E = 25.24 GPa and E = 28.85 GPa; summer bands E = 19.37 GP and E = 23.02 GPa). Young's moduli of coralline algae are notably lower than moduli measured for other biogenic calcite (brachiopods 30–60 GPa) and aragonite (coral - 60 GPa) (Denny, 2016; Perez-Huerta et al., 2008; Tanur et al., 2010). Inorganic aragonite is known to be denser, harder and less brittle than calcite (Roberts et al., 1990), so the higher values of the corals are expected (Tanur et al., 2010). Mg-calcite is meant to have higher Young's moduli than calcite, as increasing Mg content increases deformation resistance and therefore increases the elastic modulus (Ma et al., 2008; Xu et al., 2009; Zhang and Reeder, 1999). Sea urchin teeth, which have high Mg-calcite skeletons, have unusually high elastic moduli, which the authors attributed to Mg concentration, small size and their lack of orientation of the calcite crystals (Ma et al., 2008). The Mg concentration in rhodoliths are much lower than the concentrations found in the calcite of sea urchin teeth

and therefore could explain our results, although this causal relationship between elastic modulus and Mg concentration has not been proven yet in corallines.

The differences in Young's modulus between echinoderms and corallines are possibly caused by the crystal arrangement. The crystals of the polycrystalline matrix of sea urchin teeth lack orientation and are very small in size, while the teeth and plates, embedded into the matrix made up of single crystals, provide a support framework to the matrix (Ma et al., 2008). In corallines, calcite crystals are located in a mesh of organic fibrils. Crystals within the cell wall are mostly radially orientated, while the crystals within the thin middle lamellae are either orientated randomly or parallel to the filament axis (Nash and Adey, 2017a; Nash and Adey, 2017b). In corallines, the ratio of organic to carbonate changes between cell types and species, while the degree of mineralisation, which also changes between cell types and species, additionally differs within the same cell wall (Nash and Adey, 2017a; Nash and Adey, 2017b). The crystal arrangement found in sea urchins are thought to attribute to the extremely high modulus values, hence these differences in crystal arrangement between sea urchins and corallines may better explain the lower Young's modulus measured in corallines. The differences in the Young's modulus between summer and winter growth could also be explained by the crystal arrangement on the microscale. In the warmer, summer months as growth rate increases less calcite relative to cell volume is deposited (Freiwald and Henrich, 1994). This change in growth may affect the degree and nature of mineralisation and/or the ratio of organic to inorganic material on the microscale, and therefore account for the difference in Young's modulus between seasons (Perez-Huerta et al., 2008). However, this seasonal variation suggested on the microscale would need to be confirmed. We do not consider cellular structure to have an influence on the seasonal differences in the Young's moduli. Cell wall thickness, which differs between seasons, can influence the measured material properties as a thicker cell wall would have more calcite than a thinner cell wall and therefore different material properties. However, our data is based on multiple nanoscale measurements at the cellular nodes and therefore should not be affected by wall thickness. The seasonal variation apparent in the Young's modulus is small, which suggests that future changes in climate are not likely to cause large fluctuations in the Young's modulus and by extension material properties. We therefore suggest that the differences seen in the structural integrity due to changing environmental conditions (Melbourne et al., 2015; Ragazzola et al., 2012) are the result of changes in cellular structure more than the material properties.

This is the first study to measure material properties in corallines, therefore comparison with other calcifying organisms must be interpreted with caution. To have a greater understanding on how the calcified structure in corallines affects material properties a more detailed coralline study needs to be undertaken.

4.3. Structural integrity in a future world

Using our new accurate loads and material properties, the total stresses and strains experienced by the model are larger than previous model predictions (Table 3). Analysing the 95th percentile, as this excludes extreme stresses adjacent to the loads and constraints, all model stresses are lower than experimentally recorded rhodolith breaking stresses, highlighting the ideal construction of the skeleton for the dynamic environment it lives in.

Modelling the loads predicted for future extreme storm surges result in internal stresses that exceed breakage stresses for the same skeletal cell structure. This increased fracturing raises concern as the frequency (6–34%) and intensity (2–11%) of storm surges are predicted to increase (Elsner et al., 2008; Knutson et al., 2010). Increasing water velocities will increase rhodolith mobility resulting in a higher potential of collisions with the substrate or other rhodoliths, and hence amplify the problem. Therefore, we predict that increased fracturing of rhodoliths exposed to future stormier conditions will lead to rhodolith beds made up of smaller rhodoliths.

Relationships between the degree of branching and the associated biodiversity have been found within rhodoliths. In the Gulf of California, beds containing rhodoliths with larger branching densities and thallus volumes had higher abundances and diversity of cryptofauna (Steller et al., 2003). From assessment of maerl beds exposed to dredging we can infer that smaller rhodoliths will lead to a decrease in habitat complexity (Kamenos et al., 2003). Studies on temperate marine habitats have revealed that a loss in habitat complexity has led to a decrease in species richness and abundance (Airoldi et al., 2008). Within rhodolith beds lower complexity led to decreasing abundance and diversity of megafauna, though smaller and deep burrowing organisms remain unaffected (Hall-Spencer et al., 2003). The lower species richness may impact on prey availability for juvenile commercial species of fish such as cod (*Gadus morhua*) (Hall-Spencer et al., 2003). Based on this understanding of structural complexity on biodiversity, we infer that smaller rhodoliths in the future would lead to a decrease in habitat complexity that will ultimately negatively affect the abundance and diversity of some larger species.

Even though climate change will create new conditions, which will enable novel species to form habitats or do so in new regions, the general consensus is that future global change will alter and negatively affect current habitats more so than create new ones (Pörtner et al., 2014). For example, seaweed experience range shifts in response to warming; while this leads to new habitats it at the same time destroys existing ones (Lima et al., 2007). Rising sea levels can create new areas for colonisation, but will also challenge current habitats by decreasing light availability, if water depth would increase (Thorner et al., 2014). These changes, along with certain rhodoliths species increasing in calcification and growth under future CO_2 conditions (Riosmena-Rodríguez et al., 2016), makes it difficult to predict the structural integrity of rhodoliths under future conditions.

5. Conclusions

This study is the first to accurately obtain material properties for fully calcified coralline algae. This study is also a first in quantifying the hydrodynamic forces experienced by rhodoliths. The forces currently experienced by rhodoliths today are small showing the ideal structure of coralline algae in a dynamic environment. However, projections for intensity and frequency of storm surges in the future will result in an increase of forces acting on these organisms and resulting in internal stresses that exceed experimental breakage stresses. The dynamic environment will increase mobility of the rhodoliths and increase breakage through collisions with other rhodoliths and/or substrate. Jointly, this will lead to a shift to smaller rhodoliths and coralline gravels and therefore change the nature of the rhodolith beds and the organisms that live within them. However, future global change may also make currently inhabitable areas more favourable for rhodolith growth changing current distribution patterns. Changes in wave velocity, due to future global change, along with other changing environmental factors will therefore have impacts on the complex habitats these organisms form.

Supplementary data to this article can be found online at https://doi.org/10.1016/j.jembe.2017.11.007.

Compliance with Ethical Standards

The authors have no conflict of interest. Sampling of the protected species has been approved by the relevant bodies in England and Scotland.

Authors contributions

The initial concept of the manuscript was planned by Leanne

Melbourne, Daniela Schmidt and Emily Rayfield. All experiments, apart from the material testing, were carried out by Leanne Melbourne. Material testing was carried out and designed by Robert Harniman. Breakage stress, water velocity and drag experiments were designed by Mark Denny. All author's contributed to writing and editing of the manuscript. All authors have approved the final article.

Acknowledgements

We would like to thank Diana L. Steller for her advice and use of her *Lithophyllum margaritae* samples. We would also like to thank Andrew Cuff and Katherine Adena for collecting specimens of *Phymatolithon calcareum* and *Lithothamnion corallioides* from Falmouth, England. We would like to thank Jeremy Phillips for his discussions on the drag coefficient data. We acknowledge a NERC studentship award [NE/L501554/1] and the Natural History Museum, London for Leanne A. Melbourne and a Royal Society Wolfson Merit Award for Daniela N. Schmidt. We also thank the reviewers for their constructive comments.

References

Airoldi, L., Balata, D., Beck, M.W., 2008. The gray zone: relationships between habitat loss and marine diversity and their applications in conservation. J. Exp. Mar. Biol. Ecol. 366, 8–15.

Amado-Filho, G.M., Maneveldt, G., Manso, R., Marins-Rosa, B., Pacheco, M., Guimarães, S., 2007. Structure of Rhodolith Beds from 4 to 55 Meters Deep along the Southern Coast of Espírito Santo State, Brazil.

Bahia, R.G., Abrantes, D.P., Brasileiro, P.S., Pereira Filho, G.H., Amado Filho, G.M., 2010. Rhodolith bed structure along a depth gradient on the northern coast of Bahia state, Brazil. Braz. J. Oceanogr. 58, 323–337.

Biomaerl, 1999. Final Report, BIOMAERL project (Co-ordinator: P.G. Moore, Univesity Marine Biological Station Millport, Scotland), EC Contract No. MAS3-CT95-0020. pp. 1–973.

Bosence, D.W., 1976. Ecological studies on two unattached coralline algae from western Ireland. Palaeontology 19, 365–395.

Bosence, D.W., Pedley, H.M., 1982. Sedimentology and palaeoecology of a Miocene coralline algal biostrome from the Maltese islands. Palaeogeogr. Palaeoclimatol. Palaeoecol. 38, 9–43.

Carrington, E., 1990. Drag and dislodgment of an intertidal macroalga: consequences of morphological variation in *Mastocarpus papillatus* Kützing. J. Exp. Mar. Biol. Ecol. 139, 185–200.

Carro, B., Lopez, L., Peña, V., Bárbara, I., Barreiro, R., 2014. DNA barcoding allows the accurate assessment of European maerl diversity: a proof-of-concept study. Phytotaxa 190, 176–189.

Denny, M., 2016. Ecological Mechanics: Principles of Life's Physical Interactions. Princeton University Press, Princeton, New Jersey.

Dudgeon, S.R., Johnson, A.S., 1992. Thick vs. thin: thallus morphology and tissue mechanics influence differential drag and dislodgement of two co-dominant seaweeds. J. Exp. Mar. Biol. Ecol. 165, 23–43.

Dutertre, M., Grall, J., Ehrhold, A., Hamon, D., 2015. Environmental factors affecting maerl bed structure in Brittany (France). Eur. J. Phycol. 50, 371–383.

Elsner, J.B., Kossin, J.P., Jagger, T.H., 2008. The increasing intensity of the strongest tropical cyclones. Nature 455, 92–95.

Foster, M.S., 2001. Rhodoliths: between rocks and soft places. J. Phycol. 37, 659–667.

Fox, R.W., McDonald, A.T., Pritchard, P.J., 1985. Introduction to Fluid Mechanics. John Wiley & Sons, New York.

Freiwald, A., Henrich, R., 1994. Reefal coralline algal build-ups within the Arctic circle: morphology and sedimentary dynamics under extreme environmental seasonality. Sedimentology 41, 963–984.

Gaylord, B., Blanchette, C.A., Denny, M.W., 1994. Mechanical consequences of size in wave-swept algae. Ecol. Monogr. 64, 287–313.

Grall, J., Hall-Spencer, J.M., 2003. Problems facing maerl conservation in Brittany. Aquat. Conserv. Mar. Freshwat. Ecosyst. 13, S55–S64.

Halfar, J., Zack, T., Kronz, A., Zachos, J.C., 2000. Growth and high-resolution paleoenvironmental signals of rhodoliths (coralline red algae): A new biogenic archive. J. Geophys. Res. Oceans 105 (1978–2012), 22107–22116.

Hall-Spencer, J., Moore, P., 2000. Scallop dredging has profound, long-term impacts on maerl habitats. ICES J. Mar. Sci. J. du Conseil 57, 1407–1415.

Hall-Spencer, J., Grall, J., Moore, P., Atkinson, R., 2003. Bivalve fishing and maerl-bed conservation in France and the UK—retrospect and prospect. Aquat. Conserv. Mar. Freshwat. Ecosyst. 13, S33–S41.

Irvine, L.M., Chamberlain, Y.M., 1994. Volume 1 Rhodophyta Part 2B Corallinales, Hildenbrandiales. Natural History Museum, London.

Kamenos, N., Moore, P., Hall-Spencer, J., 2003. Substratum heterogeneity of dredged vs un-dredged maerl grounds. J. Mar. Biol. Assoc. UK 83, 411–413.

Kamenos, N.A., Moore, P.G., Hall-Spencer, J.M., 2004. Maerl grounds provide both refuge and high growth potential for juvenile queen scallops (*Aequipecten opercularis* L.). J. Exp. Mar. Biol. Ecol. 313, 241–254.

Kamenos, N., Cusack, M., Moore, P., 2008. Coralline algae are global palaeothermometers with bi-weekly resolution. Geochim. Cosmochim. Acta 72, 771–779.

Kamenos, N.A., Burdett, H.L., Aloisio, E., Findlay, H.S., Martin, S., Longbone, C., Dunn, J., Widdicombe, S., Calosi, P., 2013. Coralline algal structure is more sensitive to rate, rather than the magnitude, of ocean acidification. Glob. Chang. Biol. 19, 3621–3628.

Knutson, T.R., McBride, J.L., Chan, J., Emanuel, K., Holland, G., Landsea, C., Held, I., Kossin, J.P., Srivastava, A., Sugi, M., 2010. Tropical cyclones and climate change. Nat. Geosci. 3, 157–163.

Lima, F.P., Ribeiro, P.A., Queiroz, N., Hawkins, S.J., Santos, A.M., 2007. Do distributional shifts of northern and southern species of algae match the warming pattern? Glob. Chang. Biol. 13, 2592–2604.

Ma, Y., Cohen, S.R., Addadi, L., Weiner, S., 2008. Sea urchin tooth design: an "all-calcite" polycrystalline reinforced fiber composite for grinding rocks. Adv. Mater. 20, 1555–1559.

Madin, J., 2004. A mechanistic approach to understanding and predicting hydrodynamic disturbance on coral reefs. In: Department of Marine Biology and Aquaculture. James Cook University.

Marrack, E.C., 1999. The relationship between water motion and living rhodolith beds in the southwestern gulf of California, Mexico. PALAIOS 14, 159–171.

Martone, P.T., 2006. Size, strength and allometry of joints in the articulated coralline—Calliarthron. J. Exp. Biol. 209, 1678–1689.

Martone, P.T., Denny, M.W., 2008. To break a coralline: mechanical constraints on the size and survival of a wave-swept seaweed. J. Exp. Biol. 211, 3433–3441.

Martone, P.T., Kost, L., Boller, M., 2012. Drag reduction in wave-swept macroalgae: alternative strategies and new predictions. Am. J. Bot. 99, 806–815.

Melbourne, L.A., Griffin, J., Schmidt, D.N., Rayfield, E.J., 2015. Potential and limitations of finite element modelling in assessing structural integrity of coralline algae under future global change. Biogeosciences 12, 5871–5883.

Moberly, R., 1968. Composition of Magnesian Calcites of Algae and Pelecypods by Lectron Microprobe Analysis Sedimentology. vol. 11. pp. 61–82.

Nash, M.C., Adey, W., 2017a. Anatomical structure overrides temperature controls on magnesium uptake — calcification in the Arctic/subarctic coralline algae *Leptophytum laeve* and *Kvaleya epilaeve* (Rhodophyta; Corallinales). Biogeosci. Discuss. 2017, 1–40.

Nash, M.C., Adey, W., 2017b. Multiple phases of mg-calcite in crustose coralline algae suggest caution for temperature proxy and ocean acidification assessment: lessons from the ultrastructure and biomineralisation in Phymatolithon (Rhodophyta, Corallinales). J. Phycol. 53, 970–984.

Perez-Huerta, A., Cusack, M., Zhu, W., 2008. Assessment of crystallographic influence on material properties of calcite brachiopods. Mineral. Mag. 72, 563–568.

Pörtner, H.O., Karl, D., Boyd, P.W., Cheung, W., Lluch-Cota, S.E., Nojiri, Y., Schmidt, D.N., Zavialov, P., 2014. Ocean systems. In: Field, C.B., Barros, V.R., Dokken, D.J., Mach, K.J., Mastrandrea, M.D., Bilir, T.E., Chatterjee, M., Ebi, K.L., Estrada, Y.O., Genova, R.C., Girma, B., Kissel, E.S., Levy, A.N., MacCracken, S., Mastrandrea, P.R., White, L.L. (Eds.), Climate Change 2014: Impacts, Adaptation, and Vulnerability. Part A: Global and Sectoral Aspects. Contribution of Working Group II to the Fifth Assessment Report of the Intergovernmental Panel of Climate Change. Cambridge University Press, Cambridge, United Kingdom and New York, NY, USA, pp. 411–484.

Ragazzola, F., Foster, L.C., Form, A., Anderson, P.S.L., Hansteen, T.H., Fietzke, J., 2012. Ocean acidification weakens the structural integrity of coralline algae. Glob. Chang. Biol. 18, 2804–2812.

Ragazzola, F., Foster, L.C., Form, A.U., Buscher, J., Hansteen, T.H., Fietzke, J., 2013. Phenotypic plasticity of coralline algae in a high CO_2 world. Ecol. Evol. 3, 3436–3446.

Ragazzola, F., Foster, L.C., Jones, C.J., Scott, T.B., Fietzke, J., Kilburn, M.R., Schmidt, D.N., 2016. Impact of high CO_2 on the geochemistry of the coralline algae *Lithothamnion glaciale*. Sci. Rep. 6.

Rasband, W., 1997–2011. ImageJ. U.S. National Institutes of Health, Bethesda, Maryland, USA. http://imagej.nih.gov/ij/.

Rayfield, E.J., 2007. Finite element analysis and understanding the biomechanics and evolution of living and fossil organisms. Annu. Rev. Earth Planet. Sci. 35, 541–576.

Riosmena-Rodriguez, R., Woelkerling, W.J., Foster, M.S., 1999. Taxonomic reassessment of rhodolith-forming species of *Lithophyllum* (Corallinales, Rhodophyta) in the Gulf of California, Mexico. Phycologia 38, 401–417.

Riosmena-Rodríguez, R., Nelson, W., Aguirre, J., 2016. Rhodolith/Maërl Beds: A Global Perspective.

Roberts, W.L., Campbell, T.J., Rapp, G.R., 1990. Encyclopedia of Minerals. Van Nostrand Reinhold.

Samuel, L.C., Monismith, S.G., 2013. Drag coefficients for single coral colonies and related spherical objectss. Limnol. Oceanogr. Fluids Environ. 3, 173–181.

Satterthwaite, F.E., 1946. An approximate distribution of estimates of variance components. Biom. Bull. 2, 110–114.

Scoffin, T.P., Stoddart, D.R., Tudhope, A.W., Woodroffe, C., 1985. Rhodoliths and corralliths of Muri lagoon, Rarotonga, Cook Islands. Coral Reefs 4, 71–80.

Steller, D.L., 1993. Ecological Studies of Rhodoliths in Bahía Concepción, Baja California Sur, México. San Jose Stte University, pp. 101.

Steller, D.L., Foster, M.S., 1995. Environmental factors influencing distribution and morphology of rhodoliths in Bahía Concepción, BCS, México. J. Exp. Mar. Biol. Ecol. 194, 201–212.

Steller, D.L., Riosmena-Rodríguez, R., Foster, M.S., Roberts, C.A., 2003. Rhodolith bed diversity in the Gulf of California: the importance of rhodolith structure and consequences of disturbance. Aquat. Conserv. Mar. Freshwat. Ecosyst. 13, S5–S20.

Tanur, A., Gunari, N., Sullan, R., Kavanagh, C., Walker, G., 2010. Insight into the composition, morphology, and formation of the calcareous shell of the serpulid *hydroides dianthus*. J. Struct. Biol. 169, S5–S20.

Thorner, J., Kumar, L., Smith, S.D.A., 2014. Impacts of climate-change-Driven Sea level rise on intertidal rocky reef habitats will be variable and site specific. PLoS One 9,

e86130.
Vogel, S., 1984. Drag and flexibility in sessile organisms. Am. Zool. 24, 37–44.
Vosburgh, F., 1982. *Acropora reticulata*: structure, mechanics and ecology of a reef coral. Proc. R. Soc. Lond. B Biol. Sci. 214, 481–499.
Wang, R.Z., Addadi, L., Weiner, S., 1997. Design strategies of sea urchin teeth: structure, composition and micromechanical relations to function. Philos. Trans. R. Soc. Lond. Ser. B Biol. Sci. 352, 469–480.
Wilson, S., Blake, C., Berges, J.A., Maggs, C.A., 2004. Environmental tolerances of free-living coralline algae (maerl): implications for European marine conservation. Biol. Conserv. 120, 279–289.
Xu, L., Renner, J., Herwegh, M., Evans, B., 2009. The effect of dissolved magnesium on creep of calcite II: transition from diffusion creep to dislocation creep. Contrib. Mineral. Petrol. 157, 339.
Young, W.C., Budynas, R.G., 2002. Roark's Formulas for Stress and Strain. McGraw-Hill, New York.
Zhang, J., Reeder, R.J., 1999. Comparative compressibilities of calcite-structure carbonates: deviations from empirical relations. Am. Mineral. 84, 861–870.
Zienkiewicz, O., Taylor, Z., Zhu, J., 2005. The Finite Element Method: Its Basis and Fundamentals. Butterworth-Heinemann, Amsterdam.